



Charge transporting enhancement of NiO photocathodes for p-type dye-sensitized solar cells

Chih-Yu Hsu^{a,1}, Wei-Ting Chen^a, Yung-Chung Chen^a, Hung-Yu Wei^b, Yung-Sheng Yen^a, Kuan-Chieh Huang^c, Kuo-Chuan Ho^{b,c,1}, Chih-Wei Chu^d, Jiann T. Lin^{a,*}

^a Institute of Chemistry, Academia Sinica, Taipei 11529, Taiwan

^b Institute of Polymer Science and Engineering, National Taiwan University, Taipei 10617, Taiwan

^c Department of Engineering, National Taiwan University, Taipei 10617, Taiwan

^d Research Center for Applied Sciences, Academia Sinica, Taipei 11529, Taiwan

ARTICLE INFO

Article history:

Received 16 November 2011

Received in revised form 16 January 2012

Accepted 22 January 2012

Available online 1 February 2012

Keywords:

Dye-sensitized solar cell (DSSC)

Nickel oxide

P-type semiconductor

Electrochemical impedance spectroscopy

Organic sensitizer

ABSTRACT

A p-type NiO film was prepared by doctor-blading of Ni(OH)₂ paste onto FTO glass, followed by sintering at 450 °C for 30 min. The influence of nucleation condition of Ni(OH)₂ on the morphology of NiO films and consequently charge transporting behavior is investigated. A smooth and compact NiO film is obtained with smaller Ni(OH)₂ sol-gel particle size, which is confirmed by the surface topography examination. The hole transporting ability of NiO semiconductor is enhanced with such a compact film because of better interconnection between particles, as evidenced from electrochemical impedance analysis. The NiO film obtained is employed as the photocathode in p-type dye-sensitized solar cells (DSSCs) using arylamine-based dyes. The short-circuit photocurrent is two times improved to ca. 2.0 mA cm⁻² compared to rough films.

© 2012 Elsevier Ltd. All rights reserved.

1. Introduction

Since the seminal report on solar-energy-to-electricity conversion by dye-sensitized solar cells (DSSCs) in 1991 [1], the sprung up literatures in the past two decades have witnessed the promising feature and even commercialization of DSSCs. DSSCs can convert environmentally friendly solar energy at promising efficiency exceeding 11% [2,3] with low manufacturing costs and are very competitive with silicon-based solar cell [4–6]. A DSSC consists of a counter electrode, electrolyte layer, and a photoelectrode with anchoring dye molecules that harvest light. The dye-generated charge, i.e., electron or hole, injects into the photoelectrode and transports to the outer circuit for electric power supply. Therefore, efficient conductivity, sufficient dye-adsorbing sites and matched energy levels with dyes are the criteria for photoelectrodes in DSSCs.

A tandem DSSC with two complementary photoelectrodes in electric circuit is designed for improving light harvest using dyes absorbing in complementary spectral region [7–9]. TiO₂ [1–4] and ZnO [10–14] are excellent candidates as n-type semiconductors

for photoanodes. On the contrary, p-type semiconductor NiO [9] is studied intensively for photocathodes in DSSCs. The working mechanisms of these two types of photoelectrodes are different: the photoexcited dye injects an electron into the conduction band of a n-type semiconductor from its LUMO (lowest unoccupied molecular orbital), while a hole at the HOMO (highest occupied molecular orbital) is injected into the valence band of a p-type semiconductor. Up to date, the gained efficiencies of tandem DSSCs compared to single cells are still limited by the NiO electrodes despite the predicted high efficiency of 43% [15]. To enhance the efficiency of p-type DSSCs for practical application in tandem DSSCs [9,16], improving the hole injection and hole mobility on NiO and preventing intensive charge recombination with redox couple are required.

NiO was first applied on p-type DSSC in 1999 by Lindquist and co-workers [17]. Nickel acetate was hydrolyzed to form Ni(OH)₂ which was used as the precursor slurry to obtain NiO after high temperature sintering. Afterwards, there were attempts to increase the hole mobility or dye adsorbing sites of NiO for improving photocurrent. Sol-gel Ni(OH)₂ was also prepared from nickel chloride for better Ni(OH)₂ particle quality [18–21]. Later, additives were added during the sol-gel process, such as polymers [22,23] for increasing surface area to porous nanostructure film or graphene [24] for assisting conduction. Among them, addition of F108 triblock copolymer turns out to be a popular route, and good photocurrent output in p-type DSSCs can be achieved [23,25–29]. On the

* Corresponding author. Tel.: +886 2 2789 8522; fax: +886 2 2783 1237.

E-mail address: jtlin@chem.sinica.edu.tw (J.T. Lin).

¹ ISE Member.

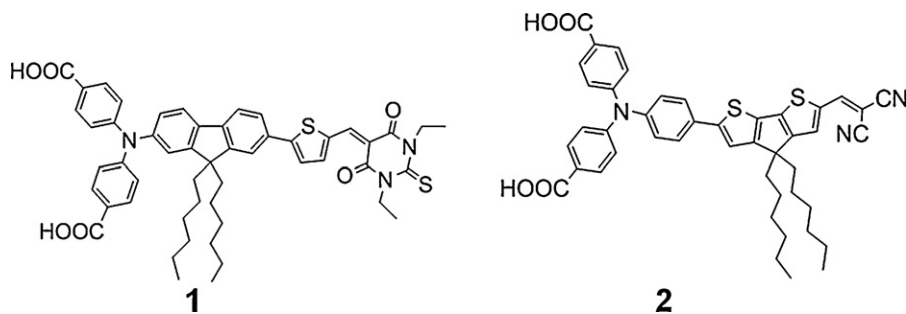


Fig. 1. Molecular structures of dye 1 and 2.

other hand, strategy towards improvement of cell photovoltage by introduction of an additional layer to retard hole recombination with redox species was reported [30–32]. There are also few reports [8,33] on commercial NiO nanopowders. Accordingly, the photovoltaic performance of mesoporous NiO film depends on the properties of NiO or Ni(OH)₂ particles on Ni(OH)₂ have shown improved electrochemical properties with a smaller crystalline size and more defects, which can be controlled by the preparation condition.

In this paper we studied the effect of particle size of Ni(OH)₂, the precursor of NiO, on NiO by varying the preparation conditions of Ni(OH)₂ particles via sol–gel process. This was paid less attention in the literature of p-type DSSCs. A substantial increase in photocurrent of the p-type DSSC can be achieved by reducing the particle size, as evidenced by the promising results using two novel arylamine-based sensitizers we developed recently (Fig. 1) [37]. The corresponding electrochemical properties and performance of p-type DSSCs will be also discussed.

2. Experimental

2.1. Preparation and characterization of NiO electrodes

The Ni(OH)₂ paste was prepared according to the commonly used sol–gel process in literatures [18–21] with some modifications. A precursor solution was prepared by adding 45 mL of aqueous solution of NaOH (1.0 M) into a 100 mL of aqueous solution of NiCl₂ (0.2 M) with vigorous stirring. The addition of NaOH_(aq.) is controlled at two extreme rates, 50 and 0.025 mL s⁻¹, namely rapid and slow, respectively, for easy realization. The morphologies of the resulting Ni(OH)₂ particles were checked by a transmission electron microscopy (TEM, JOEL JEM-1230). This solution was kept static overnight for precipitation. After removing the clear solution part, the paste was then centrifuged at 6000 rpm for 5 min and repeated for 3 times. Ethanol (30 wt.% vs. gel particles) was then added to the gel particles. Finally, ten drops (ca. 50 μL per drop) of acetic acid were added into the paste to finalize the preparation of precursor paste. The NiO films were prepared by doctor-blading the paste onto fluorine-doped SnO₂ (FTO) glass, and then sintered at 450 °C for 30 min. The film thickness was measured by a profilometer (Dektak3, Veeco/Sloan Instruments Inc., USA). The surface morphologies of the NiO films were investigated using atomic force microscopy (AFM, Digital Instrument NS 3a controller equipped with a D3100 stage) and scanning electron microscopy (SEM, Hitachi S-4700). X-ray diffraction (XRD) and X-ray photoelectron spectroscopy (XPS) were performed using a Philips X'Pert/MPD instrument (Cu Kα radiation) and a PHI 5000 VersaProbe (ULVAC-PHI, Chigasaki, Japan) system, respectively.

2.2. Device fabrication and measurement of DSSCs

The sintered NiO electrode was immersed in a 0.3 mM dye solution in THF for 16 h, where the synthetic route of the dyes is described elsewhere [37]. The counter electrodes were prepared by coating the FTO plate with H₂PtCl₆ solution (2 mM in ethanol), followed by heating at 400 °C for 15 min. The cell was assembled with the two electrodes separated by the electrolyte composed of 1.0 M of lithium iodide (LiI), 0.1 M of iodine (I₂), and 0.5 M of 4-*tert*-butylpyridine in acetonitrile and an adhered polyester tape (3 M) with thickness of 60 μm. The cell had an active area of 0.25 cm². The cell was sealing with the Torr Seal[®] cement (Varian, MA, USA). The DSSCs were energized under an Oriol Class A solar simulator (Oriol 91195A, Newport Corp.) under simulated light illumination. Light intensity at the measuring (cell) position was controlled at 1.0 sun upon calibration from an Oriol reference solar cell (Oriol 91150, Newport Corp.). Photoelectrochemical characteristics and electrochemical impedance spectra (EIS) of the NiO films or DSSCs were recorded with a potentiostat/galvanostat (CHI650B, CH Instruments, Inc., USA). The frequency range explored in impedance measurements was 10 mHz to 100 kHz with sinusoidal signal (single sine) and an ac amplitude (ΔE_{ac}) of 10 mV. The applied bias voltage was set at the open-circuit voltage of the DSSC under illumination, between the Pt counter electrode and the TiO₂-dye working electrode. As for the NiO electrodes tested in an acetonitrile solution of LiClO₄ (0.1 M), 0.0 V (vs. Ag/Ag⁺) was set in a typical three-electrode electrochemical system. The impedance spectra were fitted to an equivalent circuit model interpreting modified electrodes [38] and DSSCs [39,40], and the model parameters were obtained by ZView software.

3. Results and discussion

3.1. Ni(OH)₂ particles

As mention in Section 2, a precursor solution was firstly prepared by adding 45 mL of aqueous solution of NaOH (1.0 M) into a 100 mL of aqueous solution of NiCl₂ (0.2 M) with vigorous stirring. The pH variation during nucleation of Ni(OH)₂ resulted in structural change [36], thus the addition rate of alkaline solution was varied and checked. There was obvious difference in the TEM images (Fig. 2a and b) of Ni(OH)₂ sol–gel particles prepared from different rates. A distribution of particle size from 40 to 200 nm was found with a slow addition rate, while larger particles around 100 to 200 nm were observed in the rapid addition case. The particle size distribution is shown in Fig. 2c. It is known for a sol–gel process of metal oxides [41], condensation is facilitated in base environment due to lower surface charge and less repulsion between particles that leads to particle growth and aggregation. Thus, the particle size of Ni(OH)₂ is pH dependent and the slow addition of NaOH_(aq.) may

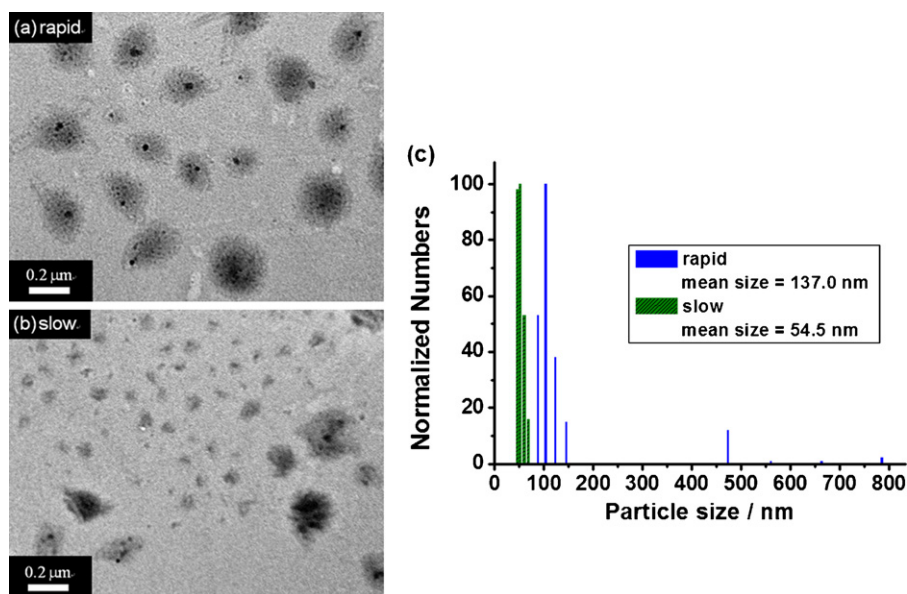


Fig. 2. TEM images of Ni(OH)₂ sol-gel particles prepared with (a) rapid and (b) slow addition rates and (c) the corresponding particle size distribution.

allow smaller Ni(OH)₂ particles. Besides, the nucleus can be clearly seen at the center of each particles from TEM images since radius growth of Ni(OH)₂ is quick and thus loose [42,43]. The particles may also aggregate from the loose structure as indicated in the ca. 470 nm peak in Fig. 2c for the rapid addition case.

3.2. NiO films

The Ni(OH)₂ paste was used to prepare NiO films on FTO glasses, herein rapid and slow films represent rapid and slow addition of NaOH solution during the formation of Ni(OH)₂ paste. Both films have an average film thickness of about 1.5 μm from the cross-sectional measurement using a profilometer as shown in Fig. 3. The film is smoother in the case of slow addition of alkaline solution as it was formed from stacking of smaller Ni(OH)₂ particles. Apparently the surface morphology of NiO films is controlled by the particle size of Ni(OH)₂. The morphology difference can be recognized from their appearance. Rough film with larger particle size leads to interference of the incident light, i.e., scattering effect. Accordingly, the rapid film looks less pervious to light and non-uniform compared to the slow film, as shown in the insets of Fig. 3. The micro-scale morphology is verified by SEM and AFM as shown in Fig. 4. The SEM image of rapid film reveals prominent aggregation between

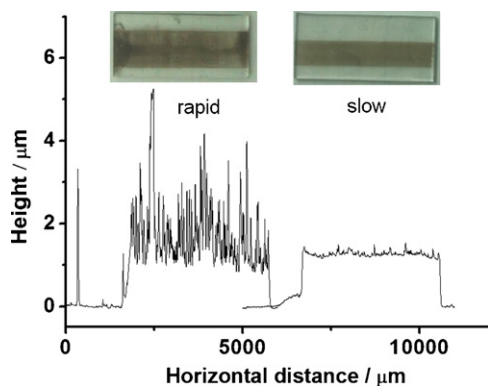


Fig. 3. Profilometer results of NiO films on FTO glasses prepared with rapid and slow addition paste. Insets show corresponding photograph.

NiO particles owing to the loose structure of the Ni(OH)₂ precursor. The stacked Ni(OH)₂ with loose periphery tends to aggregate during the pyrolysis process at high temperature sintering. Therefore, the grain particle size of NiO is larger for the rapid film (ca. 250 nm) than that for the slow film (ca. 100 nm), as evidenced from the AFM images. The roughness of these two films is also different because of different particle packing, and the root mean square roughness (R_{rms}) obtained from the AFM is 89.9 and 22.3 nm from the rapid and slow films, respectively. Thus, more smooth NiO film is obtained from relatively more compact packed film of smaller Ni(OH)₂ particles formed by a slow addition rate during the sol-gel preparation.

Fig. 5 displays XRD patterns of the rapid and slow NiO films along with a bare FTO glass as a reference. The result indicates the formation of crystalline cubic structured NiO covered on the FTO conducting glass according to (1 1 1), (2 0 0) and (2 2 0) diffractions [18]. In agreement with the morphologies observed by electron microscopes (*vide supra*), the peaks assigned to FTO (gray squares in Fig. 5) are reduced in the slow film due to the more compact coverage of NiO. The average crystalline sizes of NiO estimated by Scherrer equation are 19 and 16 nm for rapid and slow films, respectively. The crystalline size is in the same range with those studies prepared by sol-gel process in other studies [23,36]. The different Ni(OH)₂ particle size did not greatly affect the lattice size after transforming to NiO polycrystals, i.e., the crystallinity property is still identical. It implies that the different grain particle size observed from AFM is due to the aggregation of Ni(OH)₂ particles instead of the structure change after transformation from Ni(OH)₂ to NiO.

XPS spectra in Fig. 6 reveal the chemical composition of the NiO/FTO layers. The peak assigned as Sn 3d, contributed from FTO, disappeared in the slow film owing to the same reason described in the XRD part. The detection depth of XPS is about 20 angstrom while a compact coverage of NiO is about 1.5 μm. According to earlier report on NiO [44,45], the signal of Ni 2p_{3/2} is stemmed from Ni²⁺ (854.3 eV) and Ni³⁺ (857.4 eV) since both oxidized states coexist after oxidation of Ni metal. The peaks of our NiO films confirm the coexistence feature and the content ratio of these two oxidized states can be determined after Gaussian deconvolution ($R^2 = 0.926$ and 0.920 for rapid and slow films, respectively) as shown from the dotted lines in the inset of Fig. 6. The non-stoichiometric

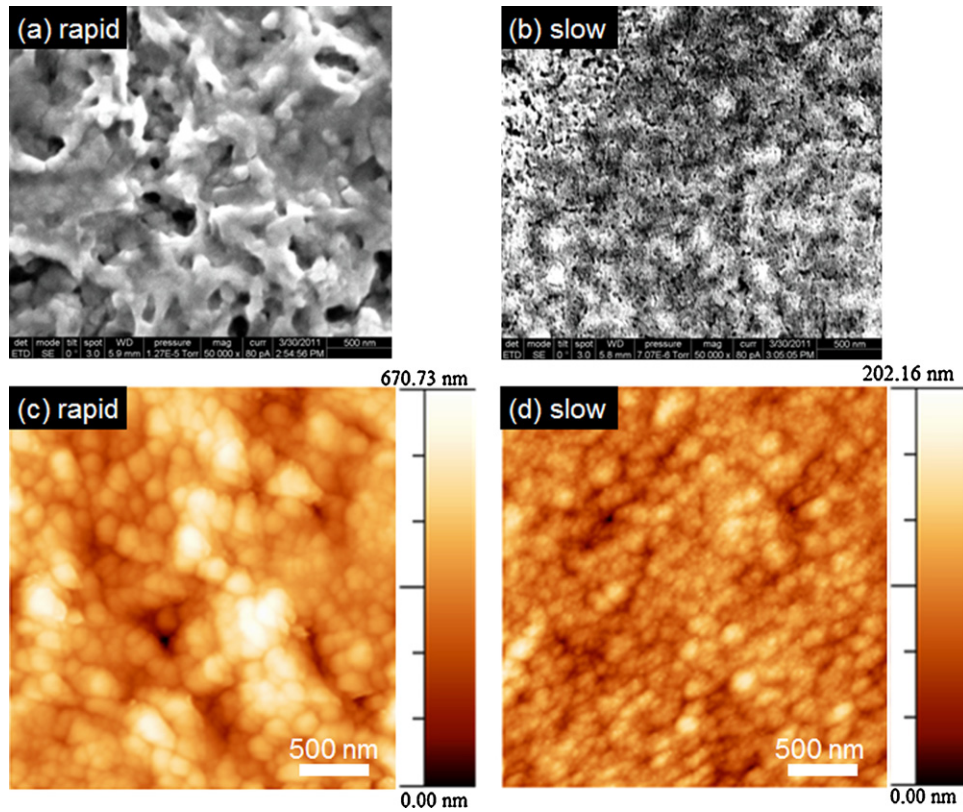


Fig. 4. Representative images of the surface morphologies of the NiO films. (a, b) SEM images of (a) rapid and (b) slow films. (c, d) Corresponding AFM images scanned in $10\ \mu\text{m} \times 10\ \mu\text{m}$ area.

composition generally known as Ni_{1-x}O [46] is calculated accordingly and x equals to 0.148 and 0.159 for rapid and slow films, respectively. For a p-type metal oxide semiconductor, it is known that the metal (cation) vacancy acts as hole hopping site. Thus, there are more nickel vacancies in the slow film according to x values, inferring a better hole transporting ability. Besides, the amounts of other cations, specifically Na^+ if any, was under detecting limit of XPS after washing $\text{Ni}(\text{OH})_2$ with deionized H_2O for 3 times (see Section 2).

The charge transporting ability of the NiO electrodes can be evaluated by the electrochemical impedance analysis at the high frequency range interpreting the charge transfer control region (Fig. 7). The rate constant of the charge transfer (k_0) can be obtained by the following equation: $k_0 = RT/n^2F^2R_{ct}AC$ [38,47], where A is the

area of the electrode, C is the bulk concentration of the ion and R_{ct} is the charge transfer resistance at the NiO layer obtained by fitting the EIS data to the equivalent circuit as shown in the inset of Fig. 7. The other symbols have their usual electrochemical meanings. The fitted R_{ct} values are 8274 and 2999 Ω for rapid and slow cases, respectively. The values of k_0 were consequently calculated as $3.22 \times 10^{-7}\ \text{cm s}^{-1}$ for the rapid film and $8.87 \times 10^{-7}\ \text{cm s}^{-1}$ for the slow film, respectively. The charge (hole) transporting ability for the slow NiO film is indeed superior to that for the rapid film. We believe that the pronounced enhancement mainly results from the compact packing which facilitates hole hopping through the nickel vacancy.

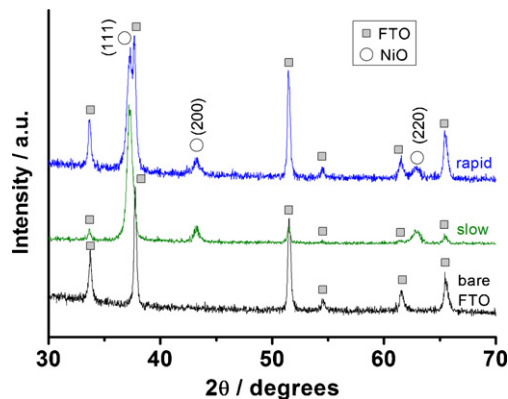


Fig. 5. XRD patterns of rapid and slow NiO films along with a bare FTO glass as a reference. Peaks of NiO are labeled as white circle while peaks of FTO, labeled as gray squares, come from the substrate.

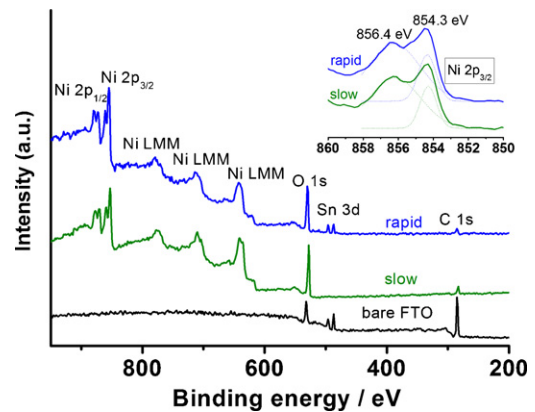


Fig. 6. XPS spectra of rapid and slow NiO films along with a bare FTO glass as a reference. The inset shows the Gaussian deconvolution results (dotted lines) of Ni $2p_{3/2}$ peaks.

Table 1
Summary of the photovoltaic performance results.

Dye	NiO photocathodes	J_{SC} (mA cm ⁻²)	V_{OC} (V)	FF	η (%)	R_{ct2} (Ω)	$C_{\mu 2}$ (mF)	τ_R (ms)
1	Rapid	0.93	0.118	0.34	0.038	259	0.58	151
	Slow	2.18	0.123	0.35	0.092	156	0.94	146
2	Rapid	0.84	0.117	0.32	0.032	219	0.60	132
	Slow	2.05	0.131	0.32	0.087	129	0.94	121

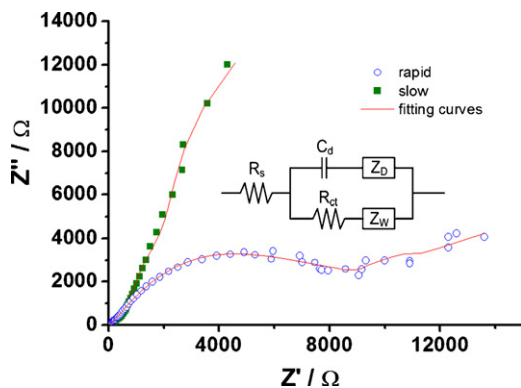


Fig. 7. EIS analysis of NiO electrodes. The inset shows the equivalent circuit describing thin-film electrodes.

3.3. DSSC performances

The corresponding two NiO films were then used as photocathodes sensitized by two novel organic dyes for a p-type DSSC and the photovoltaic J - V characteristic and EIS were analyzed. The results are shown in Fig. 8 with summarizing data in Table 1. A conspicuous difference on the photocurrent in Fig. 8a was observed for both dyes adsorbed on rapid and slow NiO films. The charge

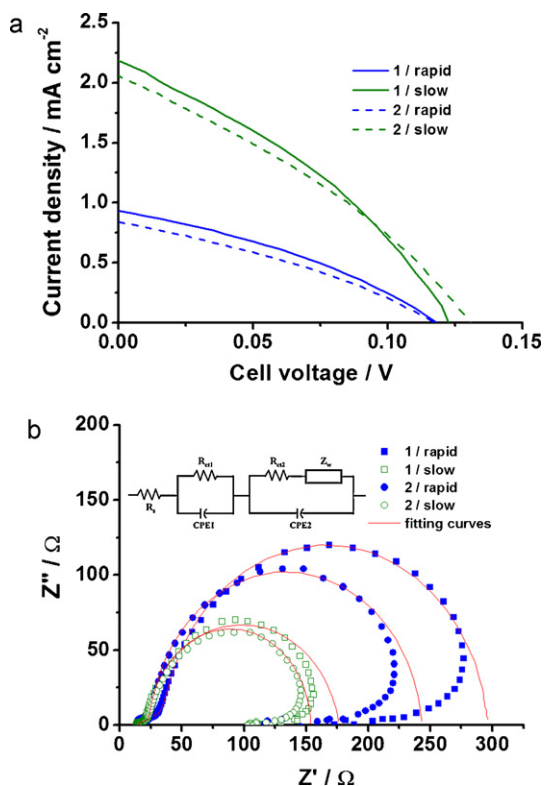


Fig. 8. (a) Photovoltaic J - V characteristics of p-type DSSCs and (b) the corresponding EIS analysis results with the equivalent circuit describing for DSSCs (inset).

transporting ability within the NiO reflects on the photocurrent. The short-circuit photocurrent of DSSCs using slow films is about two times of those using rapid films (0.94 to 2.18 mA cm⁻² for dye 1 and 0.84–2.05 mA cm⁻² for dye 2, respectively). It is in conformity with the charge transporting ability (k_0) analyses based on EIS studies (*vide supra*). A slight increase in the photovoltage of ca. 5 to 10 mV for DSSCs using slow NiO film was observed. Probably the compact NiO morphology reduced the contact between the hole and the redox mediator that changes the chemical potential of NiO. As a result, the energy conversion efficiencies enhanced from 0.038 to 0.092% for dye 1 and 0.032 to 0.087% for dye 2, respectively.

We further applied EIS technique to investigate the p-type DSSC under 1 sunlight illumination as shown in Fig. 8b. EIS is a useful technique for the analysis of charge and ionic transport processes in an electrochemical device including p-type DSSC [28]. Three semicircles are typically displayed for a DSSC structure, which are assigned to electrochemical reaction at the Pt/electrolyte (high frequency region), charge transfer at the semiconductor-dye electrode (medium frequency region) and Warburg diffusion in the electrolyte (low frequency region), as interpreted by Bisquet [48,49]. In our case, the Warburg diffusion is not obvious and negligible since we used very thin spacer (60 μ m) and low viscous solvent (0.37 cP for acetonitrile). The equivalent circuit (shown in the inset of Fig. 8b) was employed to fit the impedance spectra of the DSSCs. Meanwhile, the charge recombination lifetime (τ_R) can be obtained by $\tau_R = R_{ct2} \times C_{\mu 2}$ where R_{ct2} and $C_{\mu 2}$ represent the charge transfer resistance and the interfacial capacitance at the NiO/dye/electrolyte interface, respectively [50]. The parameters are listed in Table 1. It was found the R_{ct2} values for the DSSCs using slow films (dye 1: 156 Ω ; dye 2: 129 Ω) were indeed smaller than those using rapid films (dye 1: 259 Ω ; dye 2: 219 Ω) due to the enhanced charge transfer ability. While the interfacial capacitance for the slow films of ca. 0.94 mF is higher than that for the rapid films of ca. 0.60 mF. Likely the smaller grain particle size of the slow NiO film provide more interfaces between NiO particles, and consequently increment of the double layer capacitance. Besides, the τ_R value for the slow film is only slightly smaller than that of the rapid film. The photocurrent improvement is more likely resulted from the enhanced charge transfer ability. Accordingly, synthetic procedure of Ni(OH)₂, the precursor paste of NiO plays an important role for the quality of the NiO photocathode and therefore the performance of the DSSCs.

4. Conclusions

The growth of Ni(OH)₂ particles depends on the addition rate during sol-gel preparation: slow addition of NaOH_(aq.) into NiCl_{2(aq.)} leads to smaller particle sizes due to pH environment or local concentration of reactants during nucleation. The NiO films prepared from doctorblading Ni(OH)₂ sol-gel paste followed by a sintering process exhibit smooth and compact morphology for slow addition case. The charge transfer rate constant (k_0) of slow NiO film is 8.87×10^{-7} cm s⁻¹ which is about two times higher than that for the rapid addition case of 3.22×10^{-7} cm s⁻¹. The enhancement in the charge transporting ability is attributed to relative compact packing of NiO films. When the NiO films were used as the photocathode of p-type DSSCs and tested with two different organic

dyes, the short-circuit photocurrents of the slow NiO films were about two times improvement compared to the fast films due to smaller charge transfer resistance of the slow NiO films. Efforts on improving the hole transporting behavior of NiO should be made for enhancing the power output performance for p-type DSSCs.

Acknowledgements

We appreciate kind assistance from Mr. Chun-Chieh Wang at Department of Chemical Engineering, National Taiwan University during this work. We would like to acknowledge the Institute of Chemistry, Academia Sinica (AC), the Instrumental Center of Institute of Chemistry (AC), and National Science Council, Taiwan for financial support.

References

- [1] B. O'Regan, M. Grätzel, *Nature* 353 (1991) 737.
- [2] F. Gao, Y. Wang, D. Shi, J. Zhang, M. Wang, X. Jing, R. Humphry-Baker, P. Wang, S.M. Zakeeruddin, M. Grätzel, *J. Am. Chem. Soc.* 130 (2008) 10720.
- [3] C.Y. Chen, M. Wang, J.Y. Li, N. Pootrakulchote, L. Alababaei, C.-h Ngoc-le, J.D. Decoppet, J.H. Tsai, C. Grätzel, C.G. Wu, S.M. Zakeeruddin, M. Grätzel, *ACS Nano* 3 (2009) 3103.
- [4] J.M. Kroon, N.J. Bakker, H.J.P. Smit, P. Liska, K.R. Thampy, P. Wang, S.M. Zakeeruddin, M. Grätzel, A. Hinsch, S. Hore, U. Würfel, R. Sastrawan, J.R. Durrant, E. Palomares, H. Pettersson, T. Gruszecski, J. Walter, K. Skupien, G.E. Tulloch, *Prog. Photovoltaics* 15 (2007) 1.
- [5] M. Grätzel, *Nature* 414 (2001) 338.
- [6] M. Grätzel, *Prog. Photovoltaics* 8 (2000) 171.
- [7] E.A. Gibson, A.L. Smeigh, L. Le Pleux, J. Fortage, G. Boschloo, E. Blart, Y. Pellegrin, F. Odobel, A. Hagfeldt, L. Hammarström, *Angew. Chem. Int. Ed.* 48 (2009) 4402.
- [8] A. Nattestad, A.J. Mozer, M.K.R. Fischer, Y.B. Cheng, A. Mishra, P. Bäuerle, U. Bach, *Nat. Mater.* 9 (2010) 31.
- [9] F. Odobel, L. Le Pleux, Y. Pellegrin, E. Blart, *Acc. Chem. Res.* 43 (2010) 1063.
- [10] C. Xu, J. Wu, U.V. Desai, D.J. Gao, *Am. Chem. Soc.* 133 (2011) 8122.
- [11] Q.R. Zhang, T.R. Chou, B. Russo, S.A. Jenekhe, G.Z. Cao, *Angew. Chem. Int. Ed.* 47 (2008) 2402.
- [12] M. Law, L.E. Greene, J.C. Johnson, R. Saykally, P.D. Yang, *Nat. Mater.* 4 (2005) 455.
- [13] H.M. Cheng, W.H. Chiu, C.H. Lee, S.Y. Tsai, W.F. Hsieh, *J. Phys. Chem. C* 112 (2008) 16359.
- [14] Y.Z. Zheng, X. Tao, L.X. Wang, H. Xu, Q. Hou, W.L. Zhou, J.F. Chen, *Chem. Mater.* 22 (2010) 928.
- [15] M.A. Green, *Third Generation Photovoltaics: Advanced Solar Energy Conversion*, Springer-Verlag, Berlin, Heidelberg, 2003.
- [16] A. Hagfeldt, G. Boschloo, L. Sun, L. Kloo, H. Pettersson, *Chem. Rev.* 110 (2010) 6595.
- [17] J. He, H. Lindström, A. Hagfeldt, S.E. Lindquist, *J. Phys. Chem. B* 103 (1999) 8940.
- [18] G. Boschloo, A. Hagfeldt, *J. Phys. Chem. B* 105 (2001) 3039.
- [19] A. Morandeira, G. Boschloo, A. Hagfeldt, L. Hammarström, *J. Phys. Chem. B* 109 (2005) 19403.
- [20] P. Qin, H. Zhu, T. Edvinsson, G. Boschloo, A. Hagfeldt, L. Sun, *J. Am. Chem. Soc.* 130 (2008) 8570.
- [21] P. Qin, M. Linder, T. Brinck, G. Boschloo, A. Hagfeldt, L. Sun, *Adv. Mater.* 21 (2009) 2993.
- [22] A. Nakasa, H. Usami, S. Sumikura, S. Hasegawa, T. Koyama, E. Suzuki, *Chem. Lett.* 34 (2005) 500.
- [23] S. Sumikura, S. Mori, S. Shimizu, H. Usami, E. Suzuki, *J. Photochem. Photobiol. A: Chem.* 199 (2008) 1.
- [24] H. Yang, G.H. Guai, G. Guo, Q. Song, S.P. Jiang, Y. Wang, W. Zhang, C.M. Li, *J. Phys. Chem. C* 115 (2011) 12209.
- [25] L. Li, E.A. Gibson, P. Qin, G. Boschloo, M. Gorlov, A. Hagfeldt, L. Sun, *Adv. Mater.* 22 (2010) 1759.
- [26] P. Qin, J. Wiberg, E.A. Gibson, M. Linder, L. Li, T. Brinck, A. Hagfeldt, B. Albinsson, L. Sun, *J. Phys. Chem. C* 114 (2010) 4738.
- [27] E.A. Gibson, A.L. Smeigh, L. Le Pleux, L. Hammarström, F. Odobel, G. Boschloo, A. Hagfeldt, *J. Phys. Chem. C* 115 (2011) 9772.
- [28] Z. Ji, G. Natu, Z. Huang, Y. Wu, *Energy Environ. Sci.* 4 (2011) 2818.
- [29] L. Le Pleux, A.L. Smeigh, E.A. Gibson, Y. Pellegrin, E. Blart, G. Boschloo, A. Hagfeldt, L. Hammarström, F. Odobel, *Energy Environ. Sci.* 4 (2011) 2075.
- [30] S. Uehara, S. Sumikura, E. Suzuki, S. Mori, *Energy Environ. Sci.* 3 (2010) 641.
- [31] X.L. Zhang, F. Huang, A. Nattestad, K. Wang, D. Fu, A. Mishra, P. Bäuerle, U. Bach, Y.B. Cheng, *Chem. Commun.* 47 (2011) 4808.
- [32] Z. Bian, T. Tachikawa, S.C. Cui, M. Fujitsuka, T. Majima, *Chem. Sci.* 3 (2012) 370.
- [33] A. Nattestad, M. Ferguson, R. Kerr, Y.B. Cheng, U. Bach, *Nanotechnology* 19 (2008) 295304.
- [34] F.S. Cai, G.Y. Zhang, J. Chen, X.L. Gou, H.K. Liu, S.X. Dou, *Angew. Chem. Int. Ed.* 43 (2004) 4212.
- [35] R.S. Jayashree, P.V. Kamath, G.N. Subbanna, *J. Electrochem. Soc.* 147 (2000) 2029.
- [36] Q.S. Song, Z.Y. Tang, H.T. Guo, S.L.I. Chan, *J. Power Sources* 112 (2002) 428.
- [37] Y.S. Yen, W.T. Chen, C.Y. Hsu, H.H. Chou, J.T. Lin, M.C.P. Yeh, *Org. Lett.* 13 (2011) 4930.
- [38] F. Sundfors, J. Bobacka, A. Ivaska, A. Lewenstam, *Electrochim. Acta* 47 (2002) 2245.
- [39] L.Y. Han, N. Koide, Y. Chiba, T. Mitate, *Appl. Phys. Lett.* 84 (2004) 2433.
- [40] J.Y. Han, N. Koide, Y. Chiba, A. Islam, T. Mitate, *Comptes Rendus Chim.* 9 (2006) 645.
- [41] C.J. Brinker, G.W. Scherer, *Sol–Gel Science: The Physics: Chemistry of Sol–Gel Processing*, Academic Press, Boston, 1990.
- [42] H. Orikasa, J. Karoji, K. Matsui, T. Kyotani, *Dalton Trans.* (2007) 3757.
- [43] M.X. Peng, X.Q. Shen, *J. Cent. South Univ. Technol.* 14 (2007) 310.
- [44] C.D. Wagner, W.M. Riggs, L.E. Davis, J.F. Moulder, G.E. Muilengerg, *Handbook of X-ray Photoelectron Spectroscopy*, Perkin-Elmer, Minnesota, 1979, p. 80.
- [45] I. Hotový, J. Huran, J. Janík, A.P. Kobzev, *Vacuum* 51 (1998) 157.
- [46] K. Nakaoka, J. Ueyama, K. Ogura, *J. Electroanal. Chem.* 571 (2004) 93.
- [47] A.J. Bard, L.R. Faulkner, *Electrochemical Methods: Fundamentals and Applications*, 2nd ed., Wiley, New York, 2001.
- [48] J. Bisquert, *J. Phys. Chem. B* 106 (2002) 325.
- [49] F. Fabregat-Santiago, J. Bisquert, G. Garcia-Belmonte, G. Boschloo, A. Hagfeldt, *Sol. Energy Mater. Sol. Cells* 87 (2005) 117.
- [50] K.M. Lee, Y.C. Hsu, M. Ikegami, T. Miyasaka, K.R.J. Thomas, J.T. Lin, K.C. Ho, *J. Power Sources* 196 (2011) 2416.